LAWRENCE
LIVERMORE
NATIONAL
LABORATORY

LLNL-JRNL-450974

ON THE MECHANISM OF ANOMALOUS SLIP IN BCC METALS

L. L. Hsiung

August 24, 2010

Materials Science and Engineering: A

Disclaimer

ON THE MECHANISM OF ANOMALOUS SLIP IN BCC METALS

Luke L. Hsiung*

Lawrence Livermore National Laboratory
Condensed Matter and Materials Division
L-352, P.O. Box 808
Livermore, CA 94551-9900

Abstract - The anomalous-slip behavior of bcc metals has been studied by TEM analyses of dislocation substructures developed in a [$\bar{2}$ 9 20]-oriented Mo single crystal uniaxially compressed at room temperature to a total-strain of 0.4%. It is found that the initial dislocation lines in association with "grown-in" super-jogs can act as effective sources for the formation of both $a_0/2[111]$ (Schmid factor = 0.5) and $a_0/2[1\bar{1}1]$ (Schmid factor = 0.167) coplanar screw dislocation arrays in the $(\bar{1}01)$ primary slip plane. The interaction between the multiplied $a_0/2[111]$ dislocations and pre-existing $a_0/2[1\bar{1}1]$ dislocation segments, which block the motion of the $a_0/2[111]$ dislocations, renders the multiplication of $a_0/2[1\bar{1}1]$ dislocations and leads to the formation of $a_0/2[111]$ and $a_0/2[1\bar{1}1]$ dislocation arrays on the $(\bar{1}01)$ primary slip plane. The occurrence of $\{0\bar{1}1\}$ anomalous slip is accordingly proposed to be resulting from the mutual trapping of $a_0/2[111]$ and $a_0/2[1\bar{1}1]$ coplanar dislocation arrays on the $(\bar{1}01)$ primary slip plane, which renders a cross-slip propagation of both $a_0/2[111]$ and $a_0/2[1\bar{1}1]$ screw dislocations from the $(\bar{1}01)$ plane onto the $\{0\bar{1}1\}$ planes and thus activates the $\{0\bar{1}1\}$ <111> slip systems.

Keywords: Anomalous slip; jogged screw dislocations; coplanar dislocation arrays

1. Introduction

Computer simulations and empirical studies of the core structure of single dislocation in bcc metals over the last few decades have made enormous contributions to interpret many abnormal mechanical behaviors of bcc metals: tension/compression stress asymmetry, high Peierls (friction) stress for the motion of screw dislocations, and strong strain-rate and temperature dependence of

* Corresponding author. Tel.: +1-925 424 3125; fax: +1-925 424 3815
E-mail address: hsiung1@llnl.gov

yield and flow stresses at low temperatures [1]. However, the single-dislocation core model remains inconclusive to elucidate a peculiar anomalous slip behavior of bcc metals, which occurs on planes for which the Schmid factors are fifth and sixth in the order of largest Schmid factors for the {110} <111> slip systems, and for which the resolved shear stress is less than half that on the $(\bar{1}01)$ [111] primary system. Note that the anomalous slip behavior is also known as the violation of Schmid′s law, which states that plastic deformation of a single-crystal metals would begin on a slip system (a combination of the slip plane and the slip direction) when the resolved shear stress on the slip plane and in the slip direction reached a critical value (i.e., critical resolved shear stress). The resolved shear stress (τ) is given by $\tau = \sigma \cos \phi \cos \lambda$, where σ is applied stress, ϕ is angle between the stress axis and the normal to the slip plane, and λ is angle between the stress axis and the slip direction. The factor $\cos \phi \cos \lambda$ is usually called the Schmid factor (m). Schmid′s law in general is well obeyed by close-packed face-centered cubic (fcc) and hexagonal closed-packed (hcp) metals, which deform by slip in close-packed directions on planes that are close-packed planes. Body-centered cubic (bcc) metal is however not a close-packed structure, which deforms by slip in the most closely packed direction: <111> on a number of different planes belonging to the <111> zone such as {110} and {112} planes.

Although numerous studies have been conducted for the last four decades since Duesbery [2] first reported the occurrence of anomalous slip in Nb single crystals in 1969, see reviews of the subject in the literature [3 - 10], the governing mechanism remains elusive. Several studies [7, 10] have shown that the anomalous slip in bcc metals in general occurs in the deformation of ultrahigh-purity crystals with large sample sizes (> 3 mm) at low temperatures, and it accompanies a high work-hardening rate and fine and planar slip traces. This is in contract to a low work-hardening rate in association with coarse and wavy slip traces when the anomalous slip disappears at elevated temperatures. It is noteworthy that coarse and wavy slip traces appear when both {110} <111> and {112} <111> slip systems become operative [7]. Progress has been made recently on obtaining crucial evidence to rationalize the anomalous slip behavior of bcc metals through careful TEM observations of dislocation substructures evolved in the primary and anomalous slip planes of single-crystal Mo compressed at room temperature. Critical results are presented here to elucidate the underlying mechanism for the anomalous slip. It is noteworthy that single-crystal Mo was chosen for the study is based on the fact that {110} <111> is the only predominant slip system in Mo at room temperature [11], which is different from other bcc metals such as Fe and Ta, in which both {110} <111> and {112} <111> slip systems are operative at room temperature [12 - 14].

2. Experimental

Mo single crystals were obtained from Accumet Materials Company, NY, which were grown by a two-pass zone-refinement process. The as-received Mo single-crystals then were decarburized at 1800°C for 460 hours under an oxygen partial pressure of 2.1×10^{-6} torr, followed by a 24-hour bake at 2300°C under an ultrahigh vacuum (UHV) pressure of 10^{-11} torr. The residual resistively ratio was raised from 1890 for as-received crystals to 4458 for UHV purified crystals. Prior to a compression test, a single-crystal sample was first heat-treated at 1500 °C for 1 h, 1200 °C for 1 h, and then 1000 °C for 1 h at a vacuum of 8×10^{-11} torr. Testing of a single-crystal sample involves compressing a 5.5 mm x 5.5 mm x 15 mm sample (Fig. 1a) between two platen surfaces under precise conditions. To measure shear strain during compression, a 3-element rosette gauge was bonded in the gauge section on each side of the sample. The gauges were applied with room temperature curing epoxy adhesive. A compression test was performed on a single-crystal sample oriented with a stress axis parallel to a nominal singe-slip orientation of $[\bar{2}\ 9\ 20]$, in which the primary slip system of $(\bar{1}01)$ [111] is the only one among the twelve slip systems having a maximum Schmid factor (m = 0.5) as shown in Fig. 1b. The crystal was then compressed at a nominal strain-rate of 1 s^{-1} to approximately 0.4 % axial strain. Dislocation structures were examined using an optical microscope and a JEOL-200CX transmission electron microscope (TEM) operating at 200 KV. TEM foils were sliced from the gauge section of the tested piece with the foil sliced parallel to the $(\bar{1}01)$, the $(0\bar{1}1)$, and the (011) planes. TEM specimens were finally prepared by a standard twin-jet electropolishing technique in a solution of 75 vol.% ethanol and 25 vol.% sulfuric acid at 25 V and -10°C.

3. Results and Discussion

3.1 Stress-strain curve and slip-trace analysis

A stress-strain curve recorded from the uniaxial compression of a $[\bar{2}\ 9\ 20]$–oriented single-crystal Mo and an optical micrograph taken from two adjacent free surfaces are shown in Figs. 2a and 2b, respectively. It can be readily seen from the stress-strain curve shown in Fig. 2a that the work-hardening stage occurred immediately after yielding at a shear stress/strain of ~100MPa/0.08%; no easy-glide stage corresponding to a single-slip of the $(\bar{1}01)$ [111] primary system (m = 0.5) was observed. In addition, the optical micrographs shown in Fig. 2b reveal the formation of $(\bar{1}01)$, $(0\bar{1}1)$ and (011) slip lines according to the slip-trace analysis. Note that the

($\bar{1}01$) slip traces are barely recognizable on surface B. However, TEM images taken from a ($0\bar{1}1$)-sliced foil clearly show the appearance of both the ($\bar{1}01$) and the (011) slip bands associated with dislocation lines, which are shown in Fig. 2c together with the ($0\bar{1}1$) stereographic projection used for analyzing the slip traces.

3.2 Dislocation multiplication sources and coplanar screw-dislocation arrays

The initial dislocation structure of purified and annealed Mo crystals containing numerous isolated and bended dislocation lines with a dislocation density in the range of $10^6 \sim 10^7$ cm^{-2} is shown in Fig. 3a. Notice that numerous kink and jog segments can be seen along dislocation lines of a near-screw character. This segmental feature of dislocation lines in fact make a one-dimensional (1-D) line defect physically occupying a three-dimensional (3-D) space in a bulk crystal, as illustrated in Fig. 3b. That is, each near-screw dislocation line can be considered as a long threading dislocation with numerous segments resting on various slip planes. Since jog segments can act as effective pinning obstacles for the motion of screw dislocations, each segment portion of a threading dislocation can multiply and interact one another very differently under different straining conditions. Note that the conservative motion of a jogged screw dislocation is unlikely since screw dislocation line moves vertical to the <111> Burgers vector, but the jog segments along screw dislocation line move parallel to the <111> Burgers vector. The jogged screw dislocations in bcc metal can thus act as dislocation multiplication sources when deformed at low strain-rate conditions due to stress-induced migration and coalescence of jog segments, as illustrated in Figs. 3c and 3d. Both segment length and jog height increase as a result of the coalescence of jog segments. The jog coalescence continues until the segment length and jog height are greater than a critical length so that applied stress begins to push each line segment to precede multiple dislocation multiplication. However, dislocation dipoles can pinch off as a result of the non-conservative motion of screw dislocations when deformed under high strain-rate conditions [15]. While very few dislocation dipoles were found to form in Mo compressed under a strain-rate of 10^{-3} s^{-1} (see Fig. 3e), a significant increase of dipoles were found to form in Mo compressed under a strain-rate of 1 s^{-1} (see Fig. 3f).

Typical dislocation structures observed in foils sliced parallel to the ($\bar{1}01$), the ($0\bar{1}1$), and the (011) planes are shown in Figs. 4a - 4c, which reveal the formation of coplanar screw-dislocation arrays such that the $a_0/2[111]$ (m = 0.5) and the $a_0/2[\bar{1}1\bar{1}]$ (m = 0.167) coplanar arrays form in the ($\bar{1}$

01) primary slip plane (Fig. 4a), the $a_0/2[111]$ (m = 0.25) and the $a_0/2[\bar{1}11]$ (m = 0.287) coplanar arrays form in the $(0\bar{1}1)$ plane (Fig. 4b), and the $a_0/2[1\bar{1}1]$ (m = 0.222) and the $a_0/2[11\bar{1}]$ (m = 0.32) coplanar arrays form in the (011) plane (Fig. 4c). That is, at least six slip systems: $\pm(\bar{1}01)$ [111], $\pm(\bar{1}$ 01) $[\bar{1}1\bar{1}]$, $\pm(0\bar{1}1)$ [111], $\pm(0\bar{1}1)$ $[\bar{1}11]$, $\pm(011)$ $[1\bar{1}1]$, and $\pm(011)$ $[11\bar{1}]$ are operative in early stages of plastic deformation of $[\bar{2}\ 9\ 20]$-oriented single-crystal Mo. It is noteworthy that Schmid factor of the $\pm(\bar{1}01)$ $[\bar{1}1\bar{1}]$ slip system (m = 0.167) is only about one third that of the $\pm(\bar{1}01)$ [111] primary system (m = 0.5); the operation of such a slip system of the 10th sequence among the twelve (see Fig. 1b) obviously cannot be rationalized by Schmid′ law that predicts the operative slip systems based solely on the shear stress resolved from the applied stress. The underlying mechanism of anomalous slip in bcc metals is in fact intimately related to the formation of coplanar dislocation arrays on the ($\bar{1}01$), the $(0\bar{1}1)$, and the (011) slip planes. The mechanism of anomalous slip can be unveiled if the mechanism for the formation of coplanar dislocation arrays is realized.

It was mentioned above that the pre-existing screw dislocations associated with “grown-in” jogs can evolve from a self-pinning configuration into multiplication sources by the jog-coalescence process. Moreover, the jogged screw dislocations can also act as obstacles to impede dislocation motion, which are demonstrated in Figs. 5a – 5c. Here in Fig 5a, initially, only the $\pm a_0/2[111]$ dislocations can multiply and move on the $(\bar{1}01)$ plane due to the highest resolved shear stress. Later, motion of the array of $\pm a_0/2[111]$ dislocations are impeded and blocked at site **P** by a pre-existing $\pm a_0/2[1\bar{1}1]$ dislocation segment pinned at site **S**. Although the applied force acting on the $\pm a_0/2[1\bar{1}1]$ dislocation is initially too low to overcome the glide resistance for bowing the pinned dislocation segment, the force can effectively increase with increasing interaction force between the impeded dislocation array and the pinned $\pm a_0/2[1\bar{1}1]$ dislocation segment as a result of increasing number of dislocations move into the $\pm a_0/2[111]$ dislocation array. When the effective force increases to exceed the glide resistance required for bowing the pinned dislocation segment, a $\pm a_0/2$ $[1\bar{1}1]$ cooperative dislocation source generates, as illustrated in Fig. 5b. The simultaneous operation of the $\pm a_0/2[111]$ and the $\pm a_0/2[1\bar{1}1]$ dislocation sources on the $(\bar{1}01)$ primary slip plane result in the formation of the $\pm a_0/2[111]$ and the $\pm a_0/2[\bar{1}1\bar{1}]$ coplanar dislocation arrays, as shown in Figs. 4a and 5c. This reveals that unlike the interaction of dislocations through a mutual interception or cutting that takes place in conventional multiple-slip deformation, the coplanar dislocation arrays observed here can interact in planes that are parallel to each other. A mutual trapping of coplanar dislocation

arrays takes place when two different dislocation arrays glide in the same plane or in planes that are very close to each other. The observation of mutual trapping of screw dislocation arrays also indicate that the thermally activated cross-slip of screw dislocations in Mo, which can help by-passing the obstacles, is not prevalent at room temperature.

3.3 Formation of the <010>-type junction dislocations

Unlike the mutual interception or cutting of dislocation lines that move on the different slip planes, the motion of $\pm a_0/2[111]$ and $\pm a_0/2[\bar{1}\,1\,\bar{1}]$ coplanar dislocation arrays on the $(\bar{1}\,01)$ plane can result in not only trapping and blocking the dislocation arrays, but also the generation of $\pm a_0[010]$ junction dislocations by the reaction: $\pm a_0/2[111]$ **($\mathbf{b_1}$)** + $\pm a_0/2[\bar{1}\,1\,\bar{1}]$ (**$\mathbf{b_2}$**) $\rightarrow$ $\pm a_0[010]$ (**$\mathbf{b_3}$**), which is energetically feasible according to Frank's rule: $b_1^2 + b_2^2 > b_3^2$ [16]. The results of **g** • **b** analyses for verifying the formation of $\pm a_0[010]$ junction dislocations are shown in Figs. 6a – 6c. Here the $\pm a_0[010]$ junction dislocations can be identified using the reflection vector (**g**) of [101], which is available in the diffraction pattern of the $[\bar{1}01]$-zone. The contrast of $\pm a_0[010]$ junction dislocations, which are visible in both Fig. 6a (**g** = $0\,\bar{2}\,0$) and Fig. 6c (**g** = $1\,\bar{2}\,1$), becomes invisible in Fig. 6b when **g** = 101 and **g** • **$\mathbf{b_3}$** = 0. Likewise, the contrast of $\pm a_0/2[111]$ dislocations, which are visible in Fig. 6a (**g** = $0\,\bar{2}\,0$) and Fig. 6b (**g** = 101), becomes invisible in Fig. 6c when **g** = $1\,\bar{2}\,1$ and **g** • **$\mathbf{b}_1$** = 0. Meanwhile, the contrast of $\pm a_0/2[1\,\bar{1}\,1]$ dislocations remains visible in Figs. 6a – 6c. Although no **g** • **b** experiment was carried out to verify the formation of the <100>-type junction dislocations on the $(0\,\bar{1}\,1)$ and the (011) planes, it is anticipated that similar reactions, $\pm a_0/2[\bar{1}\,\bar{1}\,1] + \pm a_0/2[\bar{1}\,1\,\bar{1}] \rightarrow \pm a_0[100]$ on the (011) plane and $\pm a_0/2[111] + \pm a_0/2[1\,\bar{1}\,\bar{1}] \rightarrow \pm a_0[100]$ on the $(0\,\bar{1}\,1)$ plane, can also take place favorably.

3.4 Proposed mechanism for the anomalous slip

The mutual trapping and blocking of coplanar dislocation arrays and the formation of <010>-type junction dislocations can lead to not only the increase in glide resistance for dislocation motion but also the formation of dislocation pile-ups. Typical observations of pile-ups of screw dislocations on the $(\bar{1}01)$ plane resulting from either the formation of junction dislocations or the mutual trapping of coplanar dislocation arrays are shown in Figs. 7a and 7b. The observation of screw dislocation pile-ups again indicates that at room temperature screw dislocations in Mo move in a continuous fashion

and cannot cross-slip to by-pass obstacles, i.e., slip in Mo remains planar at room temperature. This in fact can lead to severe stress concentration as a result of the dislocation pile-ups. The cross-slip of screw dislocation can however take place when a stress concentration (σ^*) acting on the first screw dislocation in a pile-up array of n screw dislocations under an applied stress (σ), i.e., $\sigma^* = n\sigma$ [17], exceeds a threshold stress for cross slip at zero temperature, i.e., stress-induced cross slip.

Accordingly, the $\{0\bar{1}1\}$ anomalous slip in bcc metals can be rationalized by the collective effects of the simultaneous operation of primary and cooperative dislocation sources, the interaction of coplanar dislocation arrays, the occurrence of screw dislocation pile-ups, and the stress-induced cross slip of screw dislocations. The stress-induced cross slip renders render the propagation of $\pm a_0/2[111]$ and $\pm a_0/2[1\bar{1}1]$ screw dislocations from the primary slip planes onto the $(0\bar{1}1)$ and (011) planes and subsequently resulting in the anomalous operation of slip systems on the $(0\bar{1}1)$ and (011) planes. Accordingly, when cross slip of screw dislocations becomes prevalent at elevated-temperatures, anomalous slip diminishes since the mutual trapping and pile-ups of screw dislocation arrays become unlikely. A typical example of the cross slip of $\pm a_0/2[111]$ dislocations at local region of a $(\bar{1}01)$ slip band onto $(0\bar{1}1)$ is shown in Fig. 7c, in which TEM images were taken from a sample sliced parallel to the $(0\bar{1}1)$ plane. Here a narrow $(\bar{1}01)$ slip band, which is physically inclined to the $(0\bar{1}1)$ plane at 60°, can be seen in the lower portion that contains an array of $\pm a_0/2[111]$ dislocations traveling smoothly in the [111] direction. Some zigzag-shaped pre-existing dislocation segments, presumably $\mathbf{b} = \pm a_0/2[\bar{1}11]$, can also be seen at the surrounding region. An event of stress-induced cross slip of $\pm a_0/2[111]$ screw dislocations can be seen in the upper region of the slip band specified by a rectangular frame, in which many $\pm a_0/2[111]$ screw dislocations were observed to propagate from the $(\bar{1}01)$ slip band onto the $(0\bar{1}1)$ plane presumably caused by the pile-ups of screw dislocations on the $(\bar{1}01)$ plane, as depicted in Fig. 5. The cross slip of $\pm a_0/2[111]$ screw dislocations in turn triggers the operation of the $\pm a_0/2[\bar{1}11]$ cooperative dislocation sources and leads to the formation of the $\pm a_0/2[111]$ and $\pm a_0/2[\bar{1}11]$ coplanar screw-dislocation arrays on the $(0\bar{1}1)$ plane.

4. Conclusions

Dislocation structures formed in a high-purity Mo crystal compressed at room temperature to a total axial-strain of 0.4% have been studied to better understand the occurrence of $\{0\bar{1}1\}$ anomalous

slip in bcc metals. Single-crystal Mo was oriented with the compression axis parallel to a nominal "single-slip" orientation: [$\bar{2}$ 9 20] so that the ($\bar{1}$01) [111] slip system is the only system having a maximum Schmid factor (m = 0.5). The recorded stress-strain curve however reveals no singe-slip or easy-glide stage. The anomalous slip was observed to occur on the (011) and the (0$\bar{1}$1) planes according to the slip-trace analysis. TEM examinations of the dislocation structure in the ($\bar{1}$01) primary slip plane reveal that in addition to the operation of the ($\bar{1}$01) [111] slip system, the coplanar ($\bar{1}$01) [1$\bar{1}$1] slip system that has a much smaller Schmid factor (m = 0.167) is also operative. Similarly, the (0$\bar{1}$1) [111] slip system (m = 0.25) is cooperative with the coplanar (0$\bar{1}$1) [$\bar{1}$11] system (m = 0.287) on the (0$\bar{1}$1) plane; the (011) [1$\bar{1}$1] slip system (m = 0.222) is cooperative with the coplanar (011) [11$\bar{1}$] system (m = 0.32) on the (011) plane. The occurrence of {0$\bar{1}$1} anomalous slip in [$\bar{2}$ 9 20]-oriented Mo crystal is proposed to be resulting from the cooperative dislocation multiplication and mutual trapping of ± a_0/2[111] and ± a_0/2[1$\bar{1}$1] coplanar dislocation arrays on the ($\bar{1}$01) plane. The resulting internal-stresses render the propagation of both ± a_0/2[111] and ±a_0/2[1$\bar{1}$1] screw dislocations from the ($\bar{1}$01) plane onto the {0$\bar{1}$1} planes. In conclusion, the {0$\bar{1}$1} anomalous slip in bcc metals, in which plastic deformation is governed by long and straight screw dislocations, can be rationalized by the collective effects of (1) the simultaneous operation of primary and cooperative dislocation sources, (2) the interaction of coplanar dislocation arrays, (3) the occurrence of screw dislocation pile-ups, and (4) the stress-induced cross slip of screw dislocations. The anomalous slip behavior of bcc metals involves a deformation mechanism, which is too complicated for Schmid′s law to possibly predict.

Acknowledgements

This work was performed under the auspices of the U.S. Department of Energy by Lawrence Livermore National Laboratory under Contract DE-AC52-07NA27344. The author would like to express his gratitude to Mary LeBlanc and Dr. David Lassila for performing crystal purification and uniaxial compression experiments.

References

1. V. Vitek, Crystal Lattice Defects, **5** (1974) 1.
2. M. S. Duesberry and R.A. Foxall, Phil. Mag. **19** (1969) 501.
3. C. Bolton and G. Taylor, Phil. Mag. 26 (1972) 1369.

4. F. Louchet and L.P. Kubin, Acta Metall. 23 (1973) 17.

5. A.J. Garratt-Reed and G. Taylor, Phil. Mag. A39 (1979) 597.

6. J.W. Christian, Met. Tans. A, **14A** (1983) 1237.

7. W. Wasserbach, Phys. Stat. Sol. (a) **147** (1995) 417.

8. A. Seeger, Mater. Sci. and Eng., **A319-321** (2001) 254.

9. D.H. Lassila, M.M. LeBlanc, and M. Rhee, Mat. Res. Soc. Symp. Proc. Vol. **779**, MRS (2003) W2.9.1.

10. G. Taylor, Progress in Materials Science **36** (1992) 29.

11. R. Maddin, and N.K. Chen, Trans. AIME **191** (1951) 937.

12. D. Hull, Acta Metall., **9** (1961) 909.

13. B. Lestak, T. Libocicky, Acta Metall. **11** (1963) 1190.

14. B.L. Mordike, Z. Metallk., **53** (1962) 586.

15. L.M. Hsiung and D.H. Lassila, CMES, **3** (2002) 185.

16. C. Frank, Physica, **15** (1949), p. 131.

17. J. D. Eshelby, F. C. Frank, and F. R. N. Nabarro, Phil. Mag. **42** (1951), p. 351.

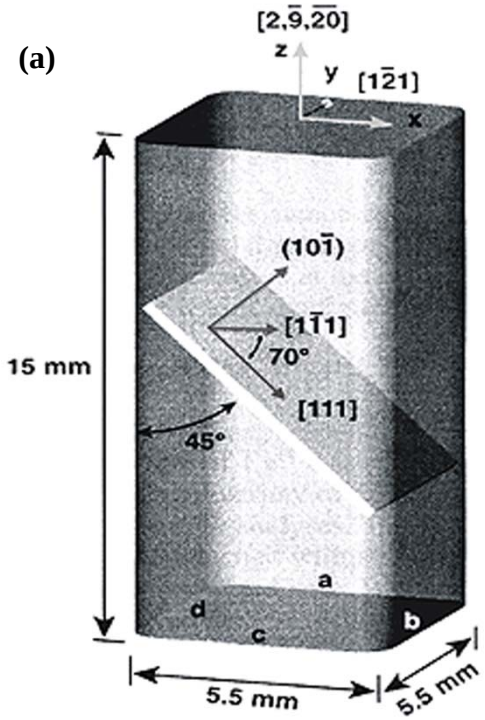

(b)

Sequence	Slip System	Schmid Factor (m)
1	$(\bar{1}01)[111]$	0.5
2	$(101)[\bar{1}11]$	0.47
3	$(011)[\bar{1}\bar{1}1]$	0.32
4	$(0\bar{1}1)[\bar{1}11]$	0.287
5	$(0\bar{1}1)[111]$	0.25
5	$(\bar{1}10)[111]$	0.25
7	$(011)[1\bar{1}1]$	0.222
8	$(101)[\bar{1}\bar{1}1]$	0.197
9	$(110)[\bar{1}11]$	0.183
10	$(\bar{1}01)[1\bar{1}1]$	0.167
11	$(\bar{1}10)[\bar{1}\bar{1}1]$	0.12
12	$(110)[1\bar{1}1]$	0.053

Fig. 1. (a) Geometry and dimension of a [$\bar{2}$ 9 20]-oriented single-crystal sample; (b) Schmid factors of the twelve {011} <111> slip systems in the single-crystal Mo with the stress-axis parallel to [$\bar{2}$ 9 20].

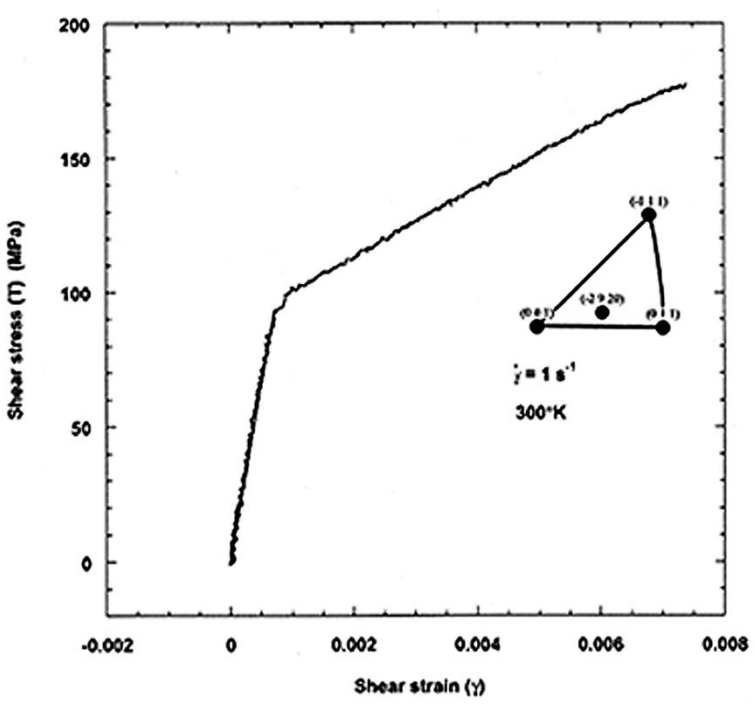

(a)

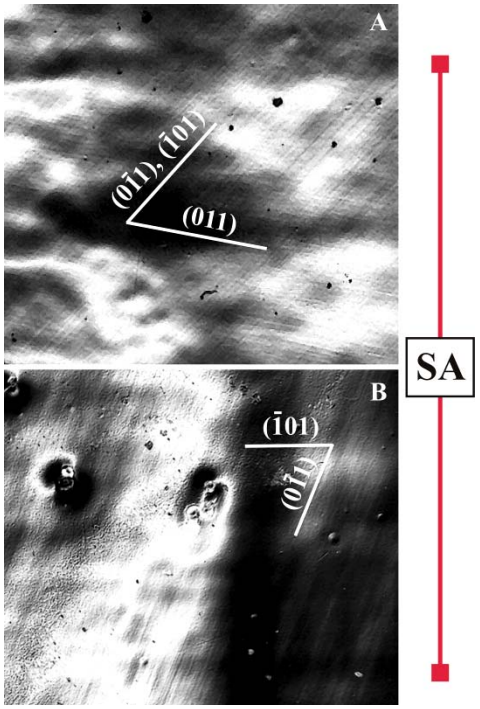

(b)

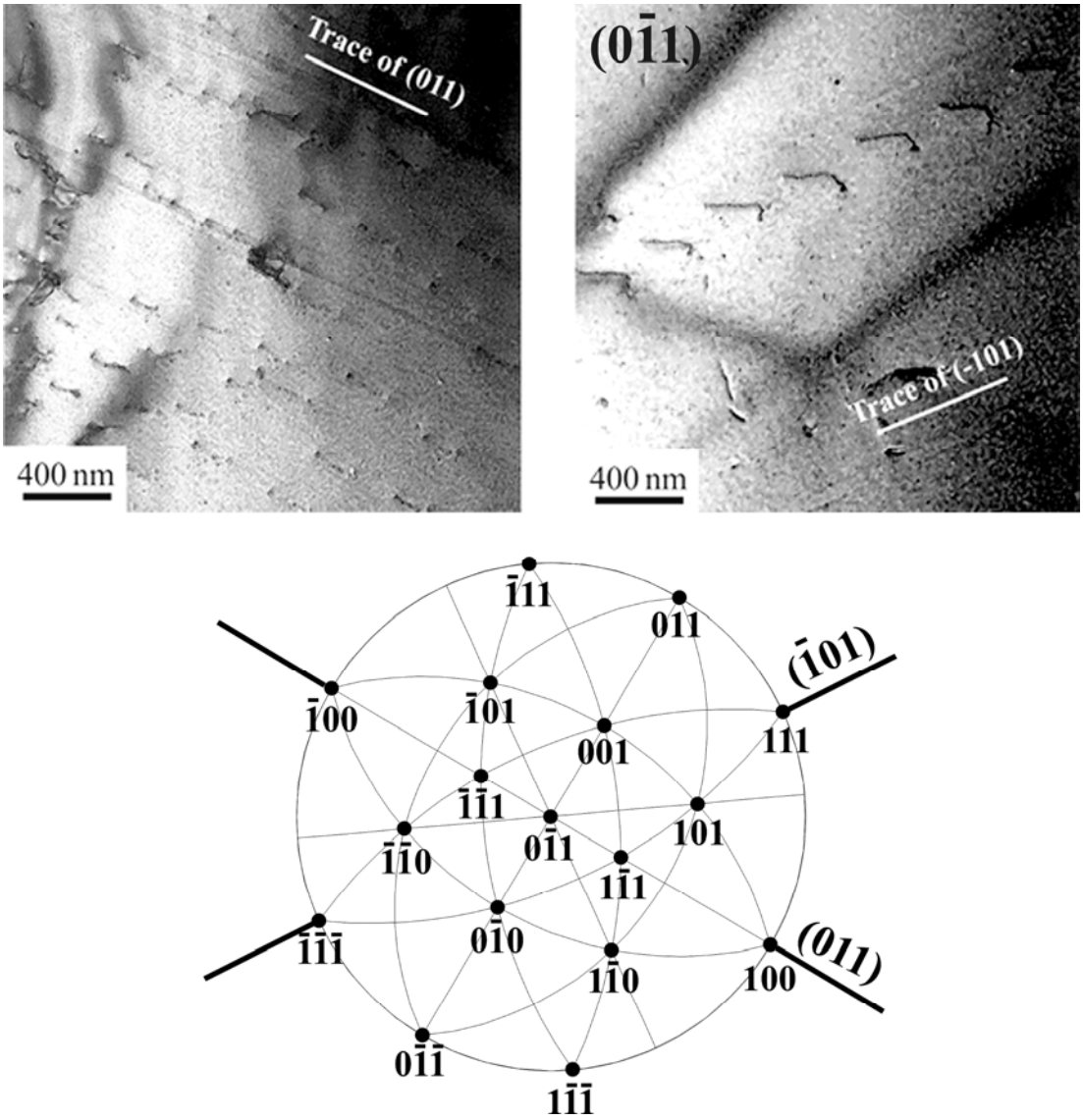

(c)

Fig. 2. (a) A stress-strain curve recorded from the uniaxial compression of a [$\bar{2}$ 9 20]–oriented Mo crystal. (b) Optical micrographs taken from two adjacent free surfaces, A: (1 $\bar{2}$ 1) and B: [49 22 -5], of the tested crystal show the occurrence of the (011) and the (0$\bar{1}$1) anomalous slip; SA stands for the stress axis, which is parallel to [$\bar{2}$ 9 20]. (c) Bright-field TEM images show both the ($\bar{1}$01) and the (011) slip bands associated with dislocation lines, which were observed in a (0$\bar{1}$1)-sliced foil; **FN** (foil normal) = [0$\bar{1}$1]. Note that the (0$\bar{1}$1) plane and the (011) plane are inclined to the (0$\bar{1}$ 1)-sliced foil at 60° and 90°, respectively.

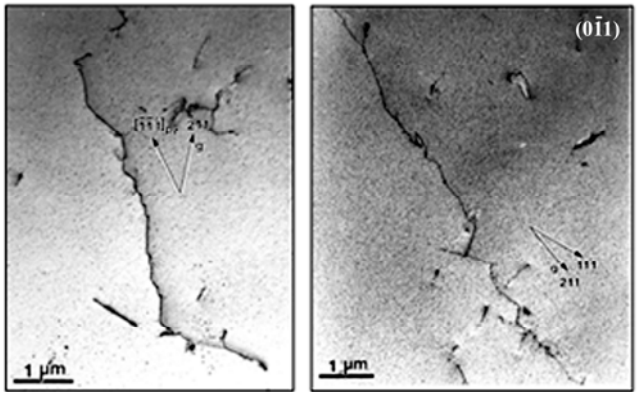

(a)

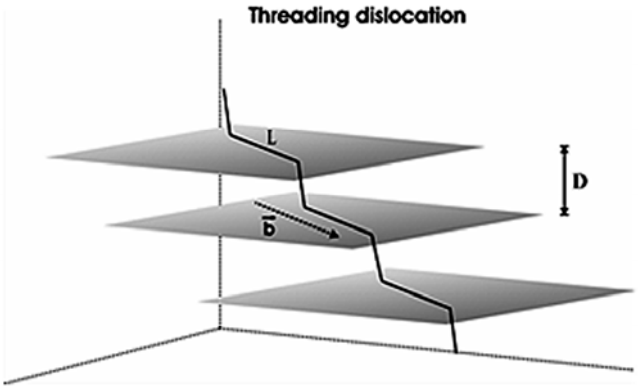

(b)

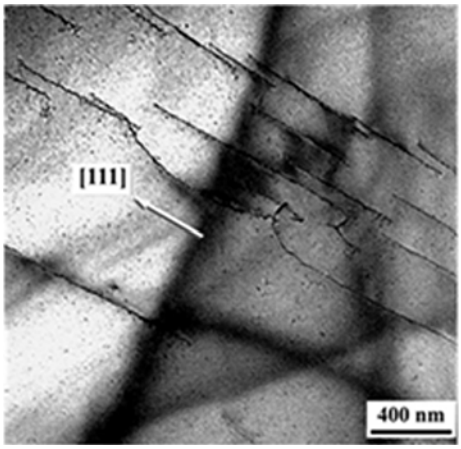

(c)

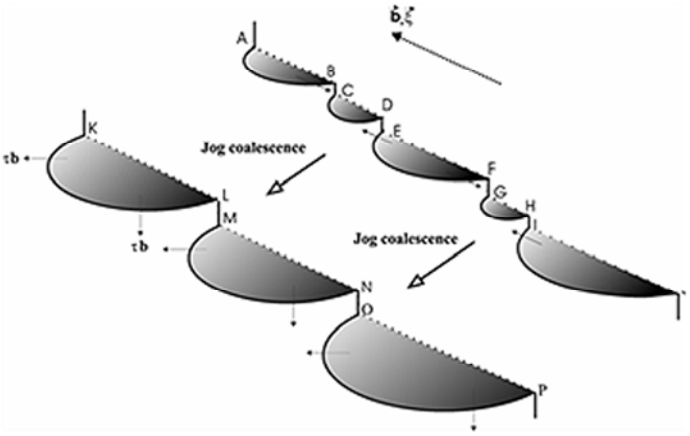

(d)

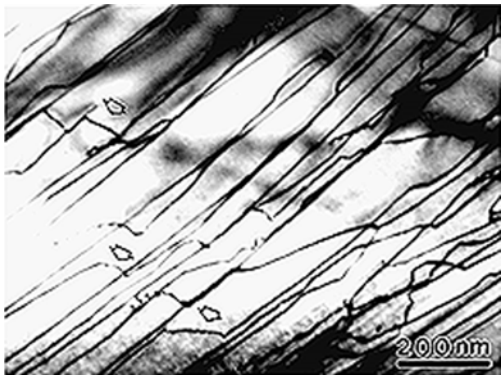

(e)

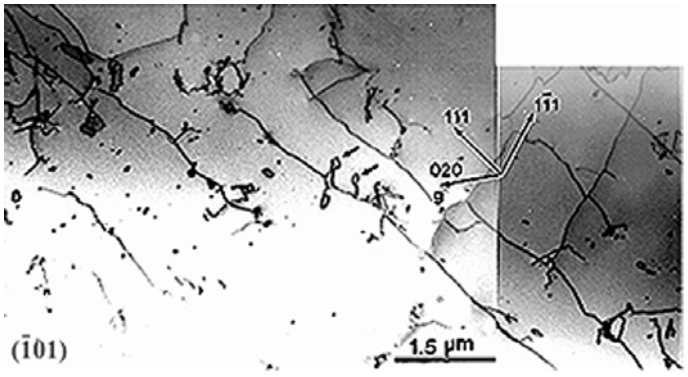

(f)

Fig. 3. (a) TEM image shows numerous kinks and jogs formed along initial dislocation lines in an as-annealed sample; (b) Schematic illustration of a jogged screw dislocation that is physically occupying a 3-D space; (c) TEM image shows the bowing of several screw dislocation segments in a deformed sample; (d) Schematic illustration of the development of multiple dislocation sources that evolve from a jogged screw dislocation through a jog coalescence process; (e) TEM image shows $a_0/2[111]$ screw dislocations associated with many super-jogs or kinks (indicated by arrows) in a sample compressed under a strain rate of 10^{-3} s^{-1} [11]; (f) TEM image shows the formation of many dislocation dipoles (debris) in a sample compressed under a strain-rate of 1 s^{-1}. Notice that two dislocation dipoles (marked by arrows) were pinching off from a screw dislocation.

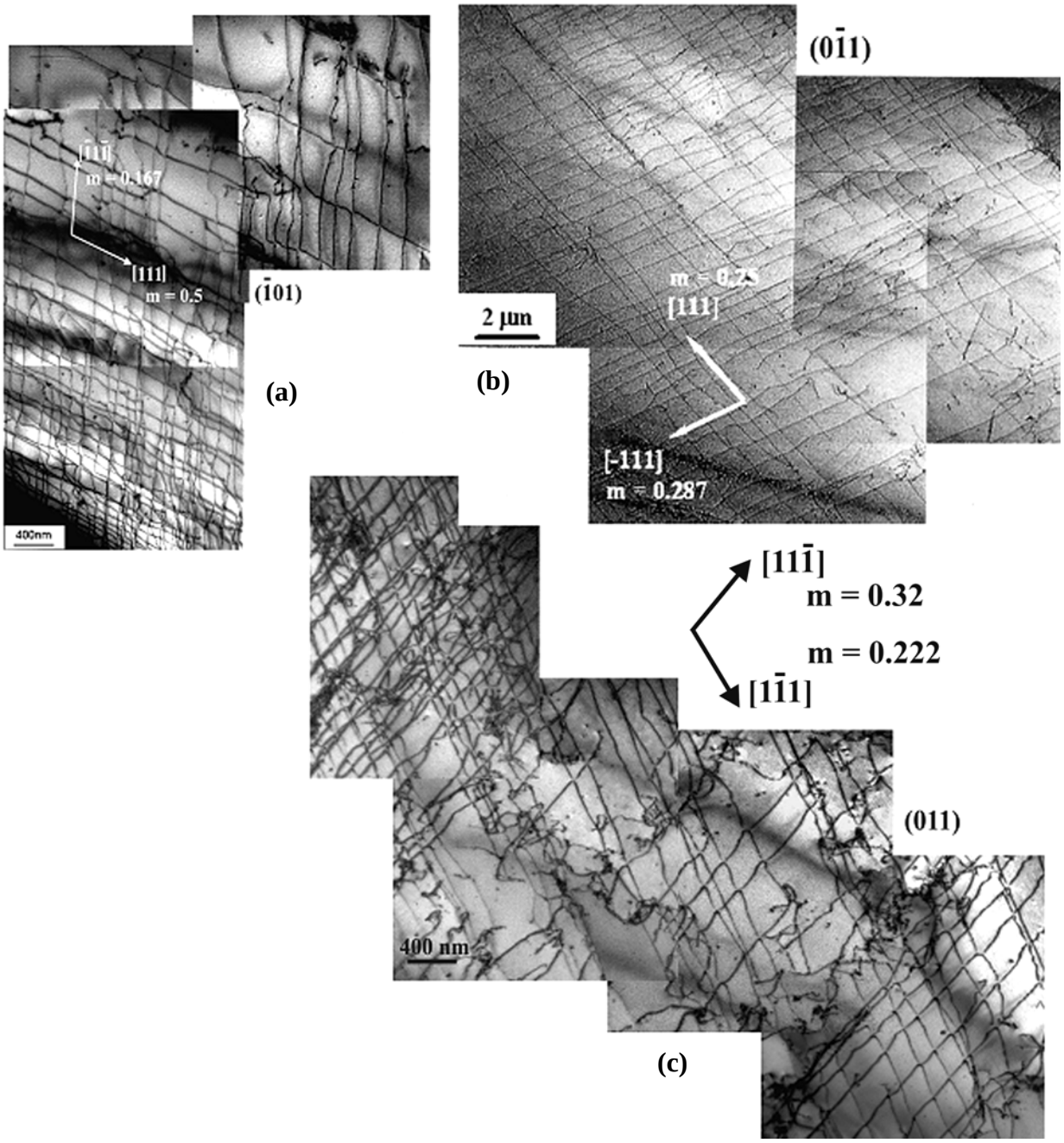

Fig. 4. TEM images taken under two-beam conditions show the formation of coplanar screw-dislocation arrays in a [$\bar{2}$ 9 20]-oriented Mo crystal compressed to 0.4% at room temperature; (a) the $a_0/2[111]$ and the $a_0/2[1\bar{1}1]$ coplanar arrays in the ($\bar{1}$01) primary slip plane, (b) the $a_0/2[111]$ and the $a_0/2[\bar{1}11]$ coplanar arrays in the (0$\bar{1}$1) plane, and (c) the $a_0/2[1\bar{1}1]$ and the $a_0/2[11\bar{1}]$ coplanar arrays in the (011) plane.

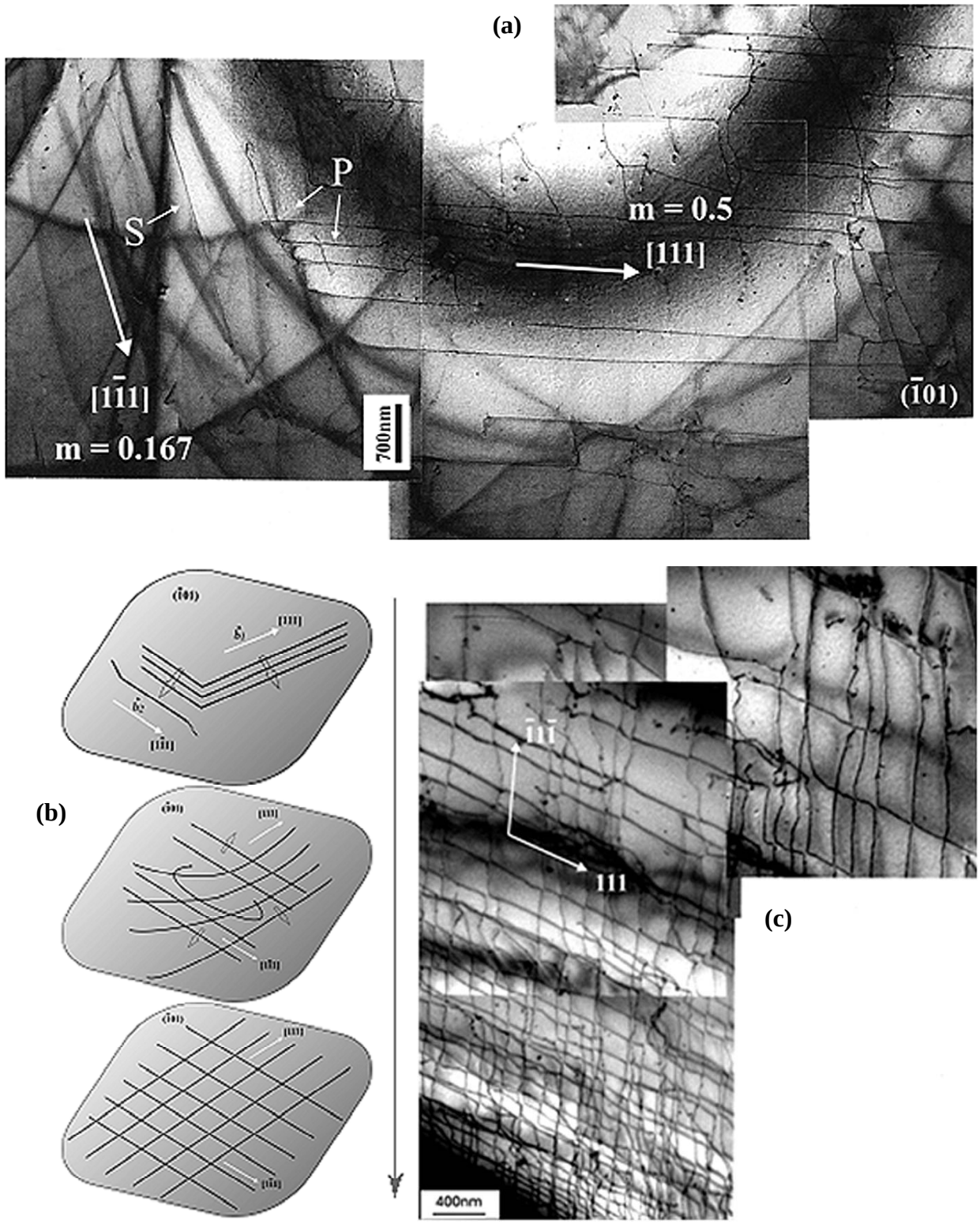

Fig. 5. (a) TEM image shows the interaction between $a_0/2[111]$ dislocation array and a $a_0/2[1\bar{1}1]$ dislocation segment; (b) A schematic representation of the cooperative multiplication of a coplanar dislocation array on the ($\bar{1}$01) plane; (c) TEM image shows the formation of coplanar dislocation arrays on the ($\bar{1}$01) plane.

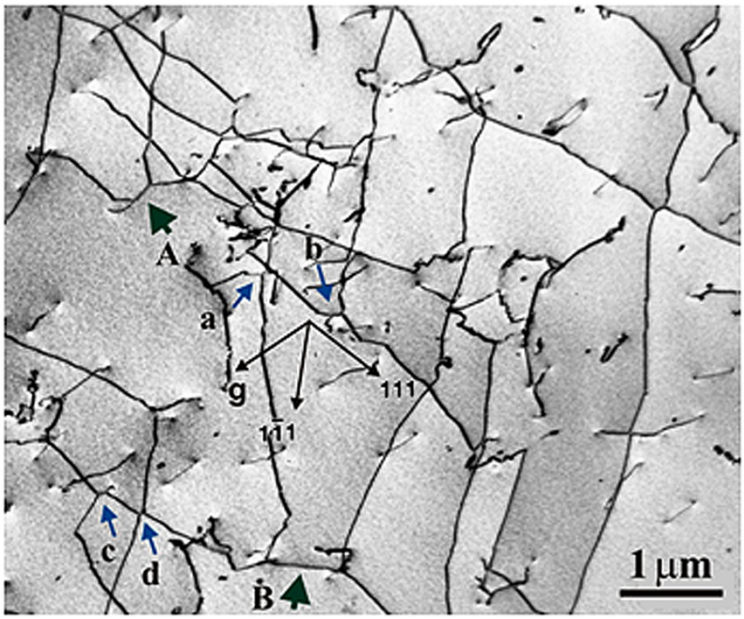

(a)

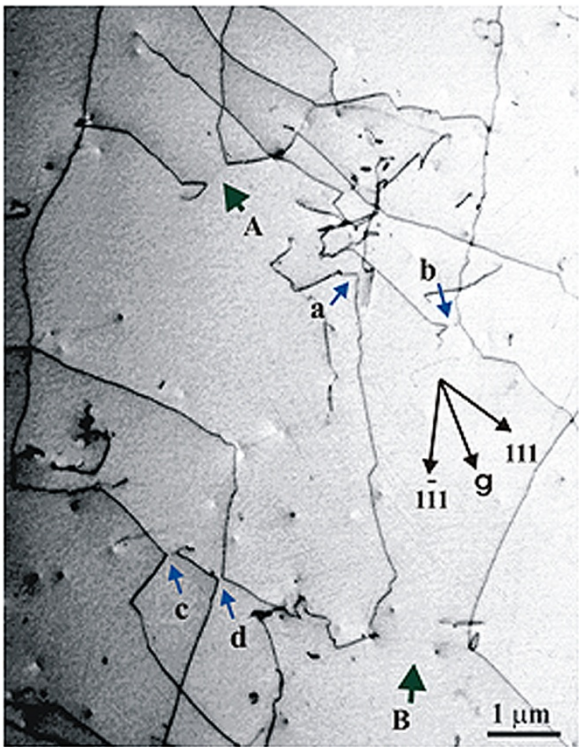

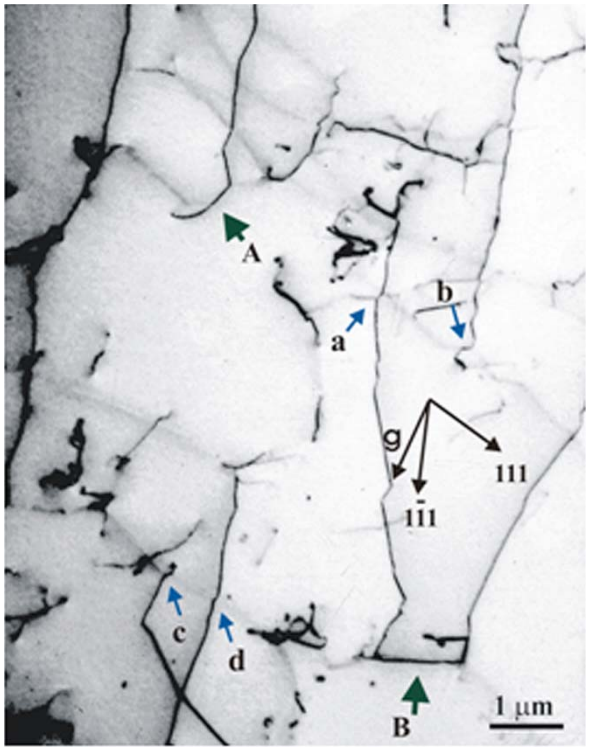

(b) (c)

Fig. 6. Two-beam bright-field TEM images obtained from the same specimen area showing the results of $\mathbf{g} \cdot \mathbf{b}$ analyses to verify the formation of the [010]-type junction dislocations in the $(\bar{1}\,0\,1)$ plane, **Z** (zone axis) ≈ $[\bar{1}01]$; (a) $\mathbf{g} = 0\,\bar{2}\,0$, (b) $\mathbf{g} = 101$, (c) $\mathbf{g} = 1\,\bar{2}\,1$. Note that the small junction dislocations are labeled by lower-case letters (a, b, c, d), and the large junction dislocations are labeled by upper-case letters (A, B).

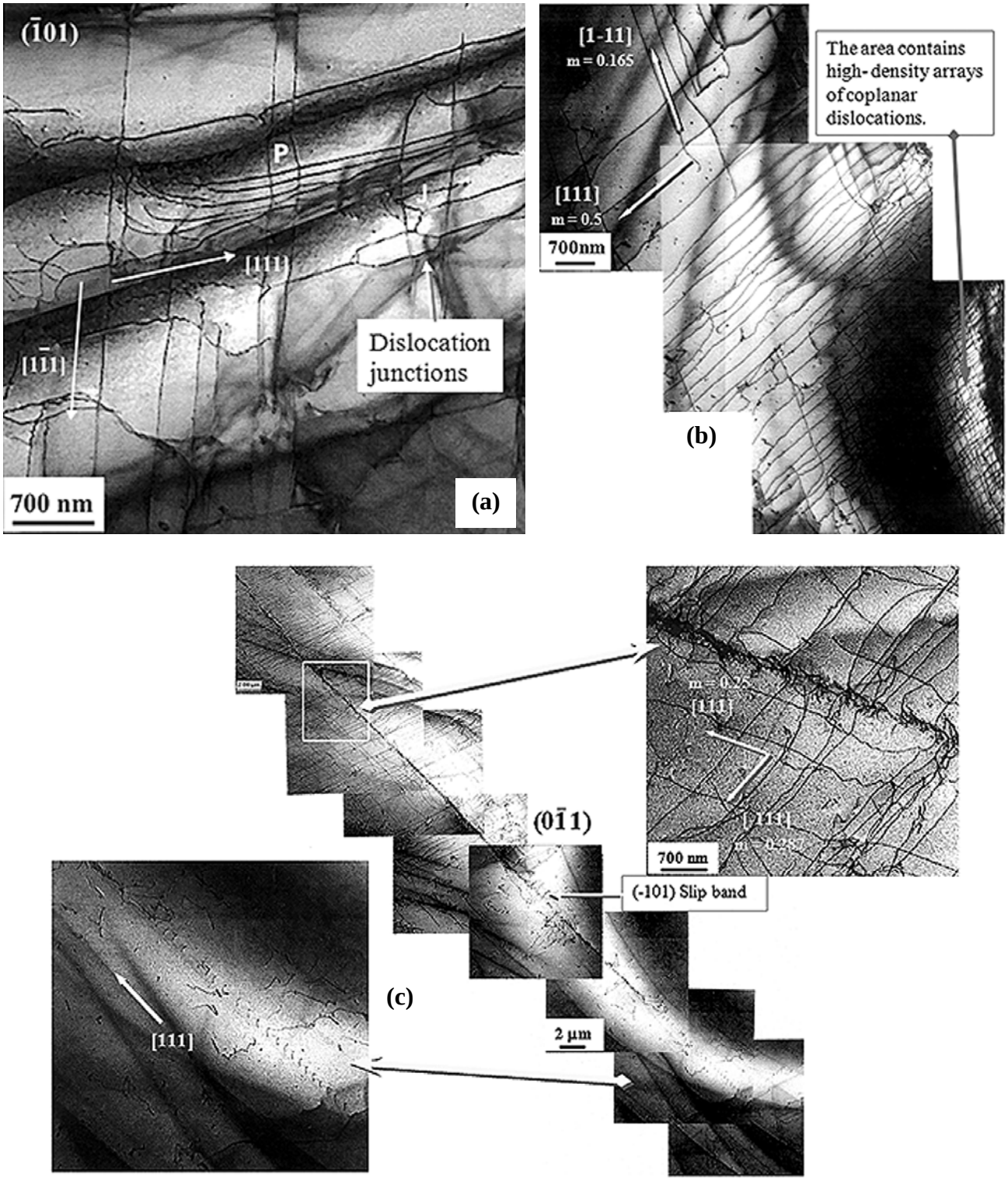

Fig. 7. TEM images show (a) the pile-up of a screw dislocation array at dislocation junctions in the $(\bar{1}01)$ slip plane, (b) the mutual trapping of two coplanar dislocation arrays in the $(\bar{1}01)$ slip plane, and (c) a cross-slip propagation of $a_0/2[111]$ dislocations from the $(\bar{1}01)$ plane onto the $(0\bar{1}1)$ plane, which was observed to occur at a local region (marked by a frame) of the $(0\bar{1}1)$ slip plane near to a $(\bar{1}01)$ slip band.